

Influence of Gd_2O_3 on thermal stability of oxyfluoride glasses

Marta Kasprzyk¹  · Marcin Środa¹ · Magdalena Szumera¹

Received: 1 December 2016 / Accepted: 24 March 2017 / Published online: 6 April 2017
© The Author(s) 2017. This article is an open access publication

Abstract The aim of the research was to determine the influence of Gd_2O_3 addition on the thermal stability of glasses from $\text{BaF}_2\text{--NaF--Na}_2\text{O--Gd}_2\text{O}_3\text{--Al}_2\text{O}_3\text{--SiO}_2$ system. Thermal analysis was carried out using DSC method. An impact of Gd_2O_3 on thermal parameters such as transformation temperature (T_g), onset temperature of crystallization (T_x), peak crystallization temperature (T_p), change of specific heat (ΔC_p) and enthalpy of crystallization (ΔH) was determined. On the basis of thermal analysis, controlled crystallization was conducted. The glass-ceramic materials were identified by XRD. Crystallization kinetics of the glasses was made on the basis of two models: Kissinger and Ozawa. Changes of the glass structure were evaluated in FTIR study. It was determined that the addition of Gd_2O_3 to the aluminosilicate glass increases the transformation temperature, simultaneously with reducing the ΔC_p and thermal stability ΔT values. It results in the decrease of ΔH . As shown, Gd significantly increases the crystallization activation energy of $\text{NaAlSi}_3\text{O}_8$. Complete substitution of Al_2O_3 with Gd_2O_3 leads to forming of $\text{Gd}_{9.33}(\text{SiO}_4)_6\text{O}_2$. Forming of Na-silicates is not observed. Because of the participation of Gd in forming of fluoride phases (BaGdF_5 , GdF_3), crystallization of $\text{Gd}_{9.33}(\text{SiO}_4)_6\text{O}_2$ is impeded.

Keywords Oxyfluoride aluminosilicate glasses · Glass-ceramics · Thermal analysis · Kinetics · Crystallization · Gd_2O_3

Introduction

More precise heat treatment than in case of oxide glasses is required to obtain transparent, low-phonon glass-ceramics based on oxyfluoride glasses [1]. It is due to the fact that introducing fluorine atoms into glass structure causes its weakening and higher ability of crystallization of oxide framework. On the other hand, the material has to maintain its transparency and luminescent properties, so that the glass-ceramics could be used as an active element in optoelectronic systems. The luminescence properties are achieved by introducing into the structure of such glass optically active lanthanides. For receiving higher luminescence efficiency and greater lifetime, the lanthanides atoms should be located in low-phonon phase, in this case the fluoride phase with higher symmetry. For this purpose, the silicate glasses doped with LaF_3 [2, 3], CaF_2 [4, 5] and BaF_2 [6, 7] were studied. The results of the research confirmed the improvement in luminescent properties of the materials. It is the issue of the material, in which the fluoride phase would readily host the optically active dopant into its structure. In this study, influence of Gd_2O_3 replacing Al_2O_3 in the glass composition on thermal glass stability and process of crystallization was studied in the $\text{BaF}_2\text{--NaF--Na}_2\text{O--Gd}_2\text{O}_3\text{--Al}_2\text{O}_3\text{--SiO}_2$ system. The crystallization process was further studied by heat treatment, followed by X-ray diffraction experiments and FTIR analysis.

Experimental

Four glasses with varying content of Gd_2O_3 were prepared using chemically pure raw materials (Table 1). The glass was melted in a platinum crucible in an electric furnace in

✉ Marta Kasprzyk
markas@agh.edu.pl

¹ Faculty of Materials Science and Technology, AGH University of Science and Technology, Mickiewicza Av. 30, 30-059 Kraków, Poland

Table 1 Nominal glass composition in mol%

| Glass code | Glass composition in mol% | | | | | |
|------------|---------------------------|--------------------------------|-------------------|-----|------------------|--------------------------------|
| | SiO ₂ | Al ₂ O ₃ | Na ₂ O | NaF | BaF ₂ | Gd ₂ O ₃ |
| FGA_0 | 50 | 10 | 15 | 10 | 15 | 0 |
| FGA_5 | 50 | 5 | 15 | 10 | 15 | 5 |
| FGA_7.5 | 50 | 2.5 | 15 | 10 | 15 | 7.5 |
| FGA_10 | 50 | 0 | 15 | 10 | 15 | 10 |

air atmosphere holding it at 1400–1470 °C for 60 min to obtain 0.1 mol of glass (ca. 10 g). During melting, the crucible was covered with a platinum plate to reduce vaporization losses. The losses of fluorides were compensated by extra amounts of components calculated from XRF analysis. The melt was poured onto a brass plate forming a layer of 2–4 mm thickness and then annealed at a temperature near the transformation temperature. The nominal glasses compositions are listed in Table 1.

Thermal stability analysis was performed with DSC method, using NETZSCH STA 449 F3 equipment and a platinum crucible in argon atmosphere. Approximately 50 mg of grounded glass below 0.06 mm were used for DSC measurement from 50 to 1050 °C. Crystallization kinetics analysis was performed for four heating rates: 5, 10, 20 and 30 K min^{−1} after appropriate equipment calibration for each rate. The transformation temperature (T_g) established on inflection point and peak temperature of crystallization (T_p) were determined from the DSC traces of the respective glasses. The activation energy (E_a) and Avrami exponent (n) were calculated according to the DSC data.

The heat treatment process was carried out in Nabertherm electric furnace. Phase identification was performed with X-ray diffraction analysis, using Philips X'Pert equipment at room temperature with CuK α radiation over the range of 10°–70° 2 θ .

The morphologies of the crystalline phases developed upon the heat treatment of bulk glass samples were examined with a scanning electron microscope (SEM, NovaNano SEM 200, FEI Company). SEM tests were performed with an attachment for the chemical analysis of specimens in micro-areas with energy dispersive X-ray spectroscopy (EDAX). The observations were carried out in the secondary electron mode in low vacuum conditions (60 Pa) and at an accelerating voltage of 18 kV. The samples were covered with a carbon layer. The chemical composition was determined using a WD-XRF Axios Max spectrometer with Rh 4 kW PANalytical lamp.

FTIR spectra were recorded with a Bruker Company Vertex 70v spectrometer. Spectra were collected in the MIR regions (2500–400 cm^{−1}) after 128 scans at 4 cm^{−1}

resolution. Samples were prepared by the standard KBr pellet method.

Results and discussion

DSC analysis

DSC analysis shows that the increasing content of Gd₂O₃ (replacing Al₂O₃) influences the thermal stability (Fig. 1). A monotonic increase in transformation temperature is observed, together with higher Gd₂O₃ content (Table 2). Difference of T_g between samples FGA_0 (with no Gd₂O₃ content) and FGA_10 (with no Al₂O₃ content) was found to be 56 °C. Jump-like change of heat capacity (Δc_p) corresponding to the transformation temperature also shows a significant modification. Addition of 5% mol Gd₂O₃ reduces it, and then, Δc_p increases along with complete replacing aluminum atoms with gadolinium. Glasses (FGA_5 and FGA_7.5) that contain both Gd and Al in their networks have the lowest Δc_p value. It is due to the fact that those glasses demonstrate lower thermodynamic fragility and are not prone to strong relaxation effects [8].

Introducing of Gd₂O₃ causes crystallization changes, such as increase in the peak crystallization temperature (T_p) with simultaneous occurrence of two exothermal effects (Table 2). Thermal stability, determined as a difference between onset crystallization temperature (T_x) and T_g [9–11], has higher values for glasses containing only one trivalent component, and this parameter has slightly lower value for glasses containing a mixture of Al₂O₃ and Gd₂O₃. Gadolinium addition also influences the crystallization enthalpy (ΔH) value. Comparing these values, it can be assumed that ΔH significantly decreases along with higher Gd₂O₃ content (Table 2). It indicates a change in mechanism of the crystallization process, associated with formation of various crystalline phases in the series of glasses, as shown in the XRD analysis.

In order to determine changes in the glasses crystallization kinetics, a non-isothermal DSC analysis was carried out with four heating rates (Fig. 1).

Crystallization kinetics analysis can be based on one of the reaction models, developed by Kissinger [12], Augis–Bennett [13] and Ozawa [14]. In the Kissinger method, the crystallization peak temperature is determined as a function of the heating rate α as following:

$$\ln(\alpha/T_p^2) = -E_a/RT_p + \text{const.} \quad (1)$$

Ozawa and Kissinger plots are commonly used to calculate the Avrami constant, n , and the crystallization activation energy, E_a , for glass [12, 15]. In the non-

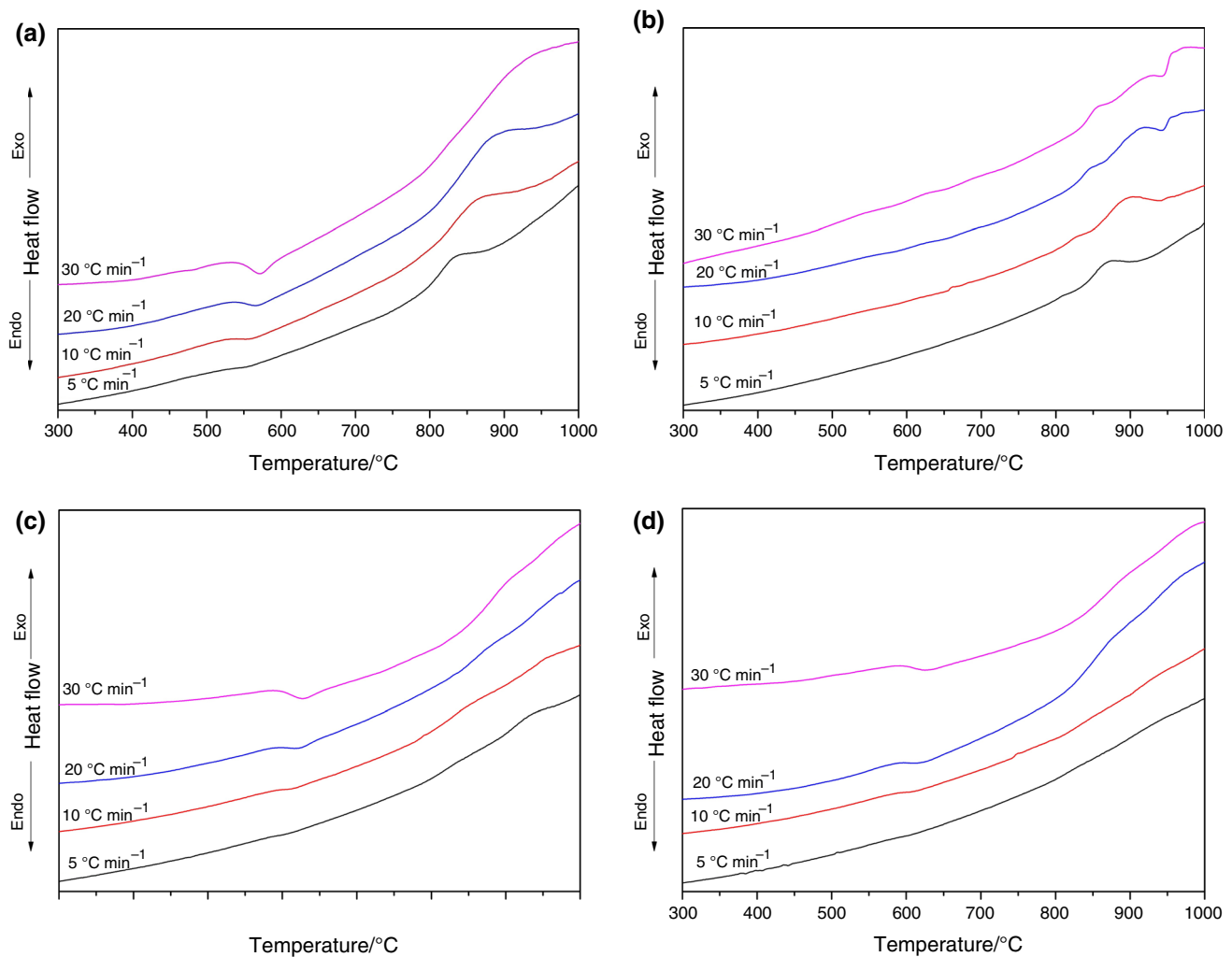


Fig. 1 DSC traces of glass: **a** FGA₀, **b** FGA₅, **c** FGA_{7.5} and **d** FGA₁₀

Table 2 Thermal characteristics of glasses from DSC curve of glass samples for $\alpha = 20 \text{ K min}^{-1}$ heating rate

| Glass code (content of Gd ₂ O ₃) | Thermal characteristics | | | | | |
|--|-------------------------|--|----------------------|-----|---------------------------------------|----------------------------|
| | $T_g/^\circ\text{C}$ | $\Delta c_p/\text{J g}^{-1} \text{K}^{-1}$ | $T_p/^\circ\text{C}$ | | $\Delta T = T_x - T_g/^\circ\text{C}$ | $\Delta H/\text{J g}^{-1}$ |
| FGA ₀ (0 Gd ₂ O ₃) | 555 | 0.16 | 890 | | 245 | 33.9 |
| FGA ₅ (5 Gd ₂ O ₃) | 580 | 0.02 | 843 | 921 | 238 | 1.2 7.3 |
| FGA _{7.5} (7.5 Gd ₂ O ₃) | 609 | 0.08 | 870 | 955 | 239 | 1.2 1.9 |
| FGA ₁₀ (10 Gd ₂ O ₃) | 611 | 0.11 | 890 | 972 | 254 | 1.1 2.2 |

T_g , transformation temperature; T_x , onset of beginning crystallization; T_p , temperature of exothermal peak; Δc_p , change of specific heat capacity at transformation region; and ΔH , crystallization enthalpy

isothermal method, the values of the Avrami parameter are determined using the Ozawa equation:

$$\ln[-\ln(1-x)] = -n \ln \alpha + \text{const.} \quad (2)$$

where x is the crystallized volume fraction at T for the heating rate α . It should be taken into account that Kissinger's

approach does not consider the concept of nucleation and growth. In this case, transformation under non-isothermal condition is described as a first-order reaction.

Figure 2 represents the relation of $\ln(T_p^2/\alpha^n)$ to $1000/T_p$ according to the Kissinger–Matusita model [12, 16, 17] which is described as:

$$\ln(T_p^2/\alpha^n) = -mE_a/RT_p + \text{const.} \quad (3)$$

In our calculation, we assume the variable amount of nucleuses due to the process of formation fluorides as the first stage of the network rearrangement according to the XRD results. They can act as a new center of nucleation of silicates. In this case, $m = n - 1$. The obtained values have good linear correlation. The effect of crystallization was not observed for FGA_10 at heating rate of 5 and 10 °C min⁻¹ and could not have been taken to our calculation. Thus, the values of E_a and Avrami parameter (n) cannot be estimated exactly for the glass and may deviate from the proper value. It is presented as the dotted line in Figs. 2 and 3.

The crystallization activation energy, determined on the basis of the plots, is presented in Table 3. Analysis of crystallization kinetics from curves according to Eq. (3) indicates that the activation energy for aluminosilicate glass (FGA_0) is slightly higher than Si–O bond dissociation energy (360–430 kJ mol⁻¹) in silicate glasses [18]. It may be connected with Al₂O₃ as a next component of the framework. There are enough modifier ions to compensate electric charge to form tetrahedral [AlO₄]. The significant higher values are obtained when Gd₂O₃ was substituted Al₂O₃. The activation energy for the precipitation of BaF₂ and BaGdF₅ is much lower (250–350 kJ mol⁻¹) [19] than those obtained in our analysis. As fluoride phases form during crystallization, Si–O bond dissociation is not actually necessary, as fluoride is not bound to silicon [20]. That is why it can be assumed that obtained in the study values apply to aluminosilica oxide network crystallization. On the DSC curves, a separate peak corresponding to fluoride phase forming was not observed. This statement is based on the XRD analysis which confirmed the fluoride crystallize below 800 °C and there is no deflection on the

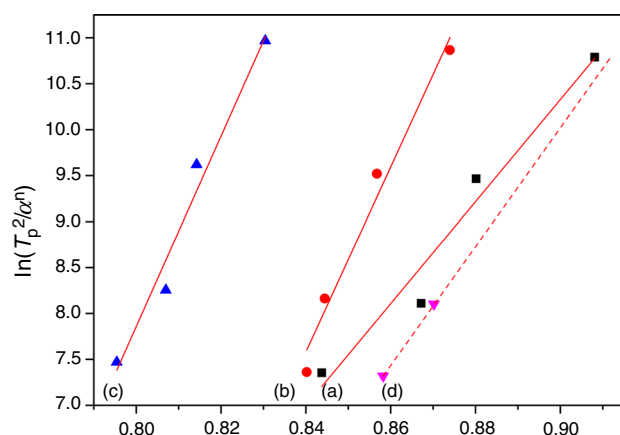


Fig. 2 Plots of $\ln(T_p^2/\alpha^n)$ versus $1000/T_p$ for the oxyfluoride glasses: *a* FGA_0, *b* FGA_5, *c* FGA_7.5 and *d* FGA_10

derivative DSC curves in the temperature region between T_g and 800 °C. However, crystallization of fluoride phases can impact the increase in crystallization activation energy of silica network by shortage of cations necessary for silicates crystallization and/or by reinforcement of the oxide framework.

The values of n determined from $\ln[-\ln(1-x)]$ versus $\ln \alpha$ plot slope (Fig. 3) are listed in Table 3. It is evident that it ranges from 1.7 to 1.4, which suggests a change in the crystallization mechanism [21]. Moreover, the calculated values of n are not integers, which indicates a multistage mechanism of crystallization and a complex crystallization behavior (Fig. 4). Silicate crystallization is preceded by fluoride phase crystallization as XRD analysis showed. It can be a result of higher chemical affinity of modifiers ions toward fluorine and lower strength of fluorine bonds than oxygen. Size and amount of formed fluorides can influence the silicate crystallization mechanism. The results suggest that with increase in Gd₂O₃ content in the glass, the crystallization mechanism changes from two-dimensional to one-dimensional growth of silicates (n parameter is lowering).

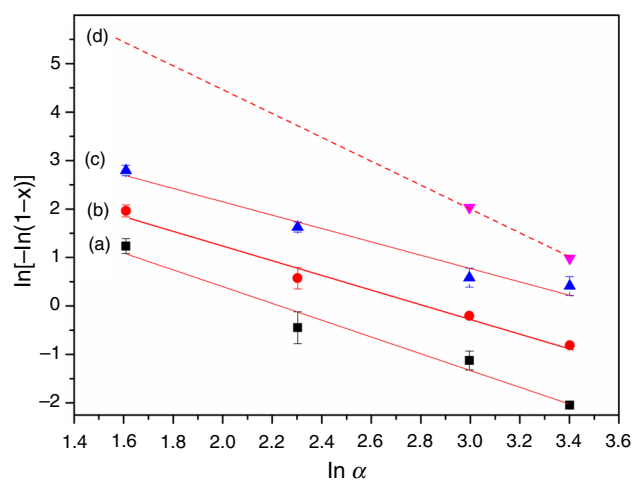


Fig. 3 Plot of $\ln[-\ln(1-x)]$ versus $\ln \alpha$ for the glasses: *a* FGA_0, *b* FGA_5, *c* FGA_7.5 and *d* FGA_10

Table 3 Activation energy of crystallization and Avrami parameter ' n '

| Glass code | Kinetics | |
|------------|--------------------------|----------|
| | $E_a/\text{kJ mol}^{-1}$ | n |
| FGA_0 | 461 ± 7 | 1.73 |
| FGA_5 | 837 ± 11 | 1.51 |
| FGA_7.5 | 862 ± 12 | 1.38 |
| FGA_10 | 545^a | 2.59^a |

^a Values were obtained only from two points on the plot

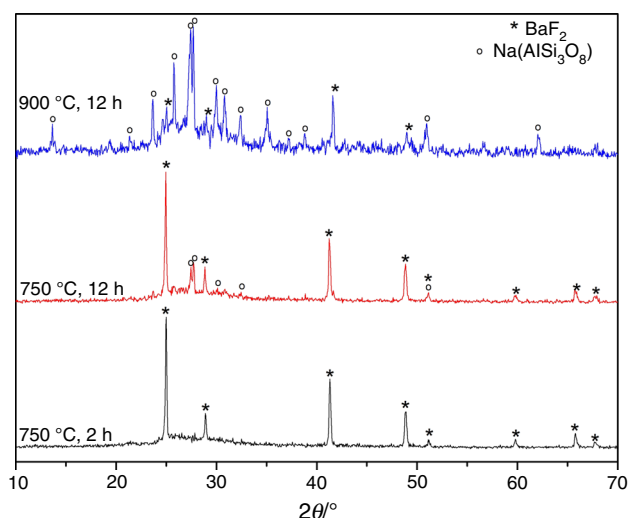


Fig. 4 XRD patterns of FGA_0 sample after heat treatment

Because of the crystallization effect disappearance in case of FGA_10 sample heated with 5 and 10 °C min^{-1} rate, it was impossible to carry out a precise crystallization kinetics analysis of this glass; thus, the E_a and n values estimated based only on two heating rates can be inaccurate. However, a lower value of crystallization activation energy and Avrami parameter, n , can be observed. These changes, as well as Δc_p , ΔT and n values, are similar to those corresponding to FGA_0. It indicates a similar role of Gd_2O_3 and Al_2O_3 in the glass structure. Their mutual substitution in the glass affects the change in thermal stability of silicate network, which must carry modification of crystallization process.

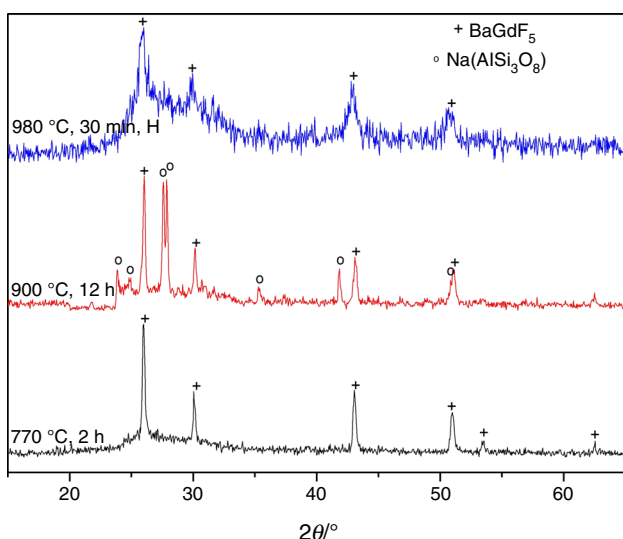


Fig. 5 XRD patterns of FGA_5 sample after heat treatment (H index indicates the sample was put into a hot furnace directly)

XRD analysis

XRD analysis revealed FGA_0 glass crystallization as a two-stage process. Heat treatment of the glass at 750 °C for 2 h leads to BaF_2 formation as a first phase (Fig. 4). This effect is not visible on DSC curves, where the crystallization effect is situated above 800 °C . The sample analysis after 12 h of heat treatment at the same temperature shows the oxide network crystallization and formation of $\text{NaAlSi}_3\text{O}_8$ (Fig. 4). Intensity of the peaks corresponding to this phase is low, which indicates the initial stage of crystallization process of this phase. Heat treatment at 900 °C for 12 h leads to BaF_2 phase disappearance

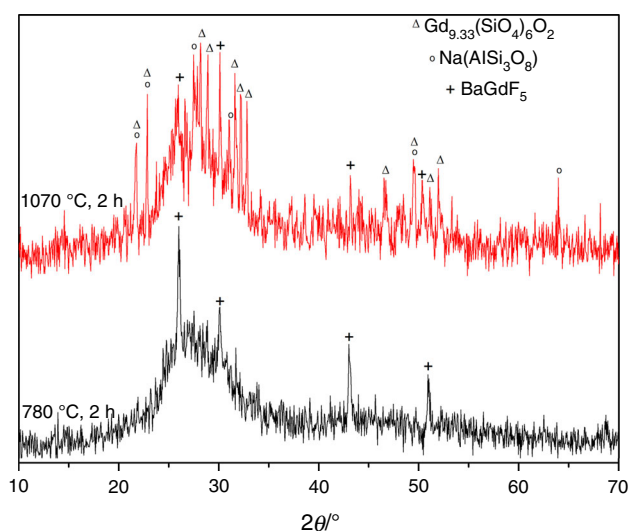


Fig. 6 XRD patterns of FGA_7.5 sample after heat treatment

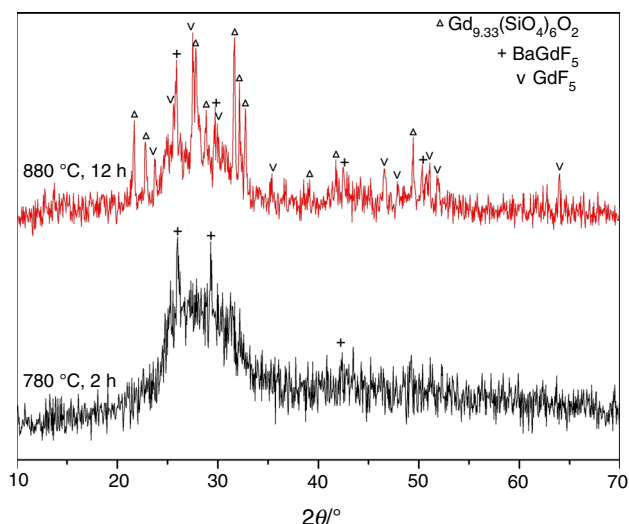


Fig. 7 XRD patterns of FGA_10 sample after heat treatment

(Fig. 4). It could be the effect of fluoride phase dissolution in the glass that becomes a melt in this temperature.

In the case of FGA_5 glass, at the first stage of crystallization (heat treatment at 770 °C for 2 h), BaGdF₅ is formed (Fig. 5). Unlike BaF₂, its thermal stability is higher

and it is not disappearing after heat treatment at 900 °C for 12 h (Fig. 5). At the same time, similarly to FGA_0 glass, the silicate network glass crystallization in the form of albite is observed (Fig. 5). To determine the effect of heat treatment procedure on both phases crystallization ability,

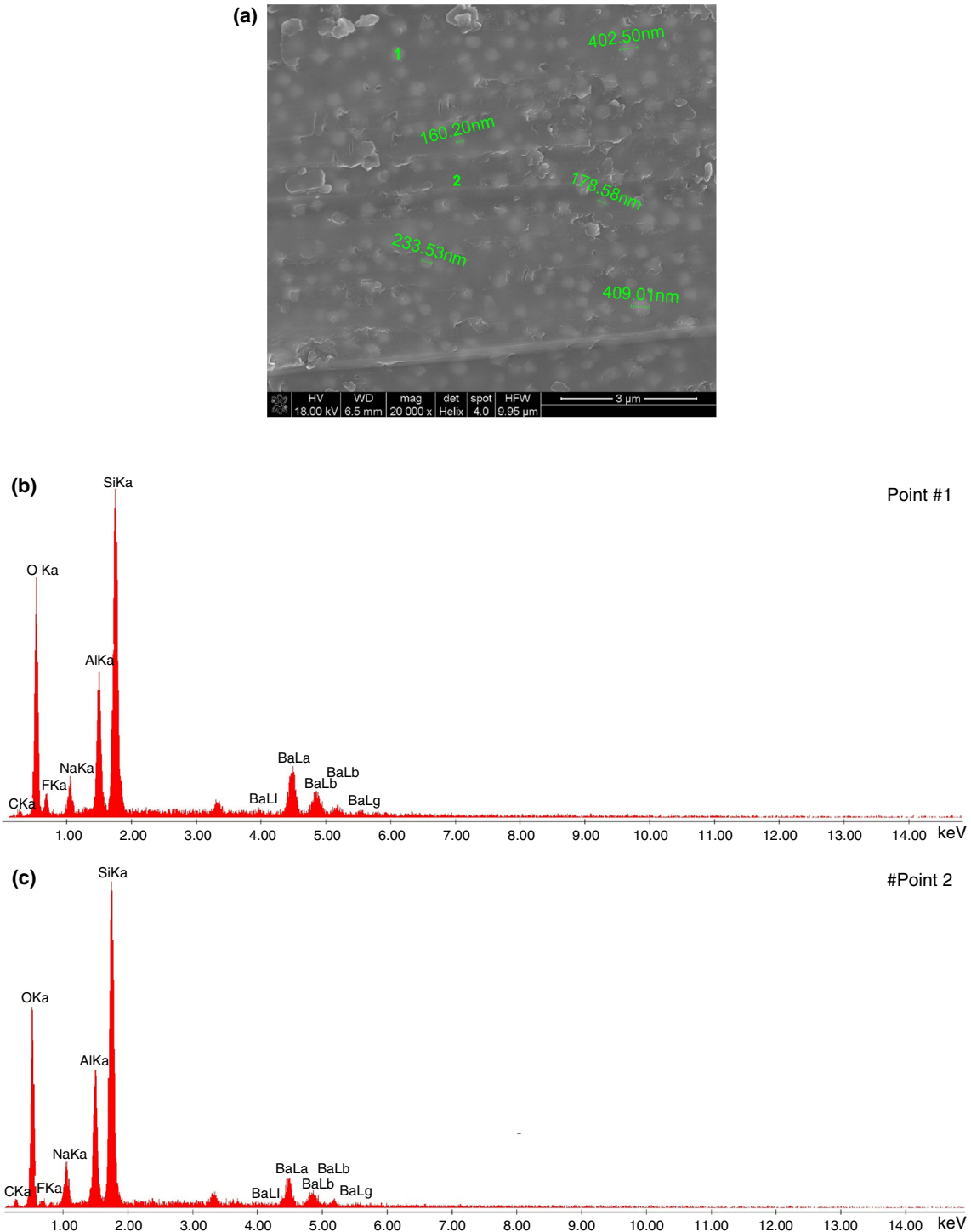


Fig. 8 SEM image (a) and EDS spectrum of FGA_0 after heat treatment at 750 °C for 2 h representing the point #1—crystallites of BaF₂ (b) and point #2—glassy matrix (c)

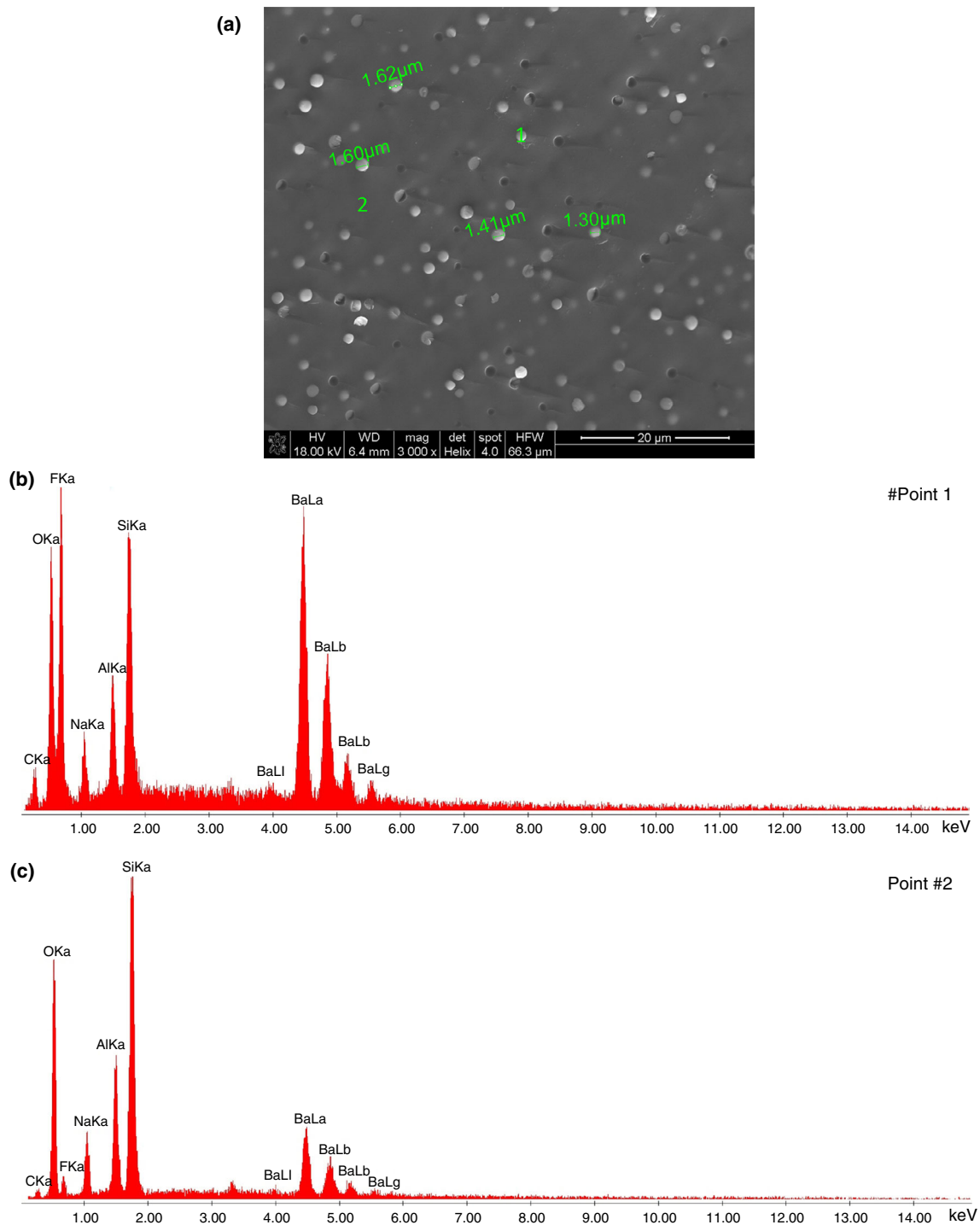


Fig. 9 SEM image (a) and EDS spectrum of FGA_0 after heat treatment at 900 °C for 30 min representing the point #1—crystallites of BaF_2 (b) and point #2—glassy matrix (c)

an experiment was conducted, in which a glass sample was placed in the preheated to 980 °C furnace and crystallized for 30 min. XRD analysis showed that under these thermal conditions, only BaGdF_5 was formed (Fig. 5). Such behavior of BaGdF_5 allows to modify the treatment process in order to obtain a transparent glass-ceramics. It is very

important, since it gives a better opportunity to control shape and size of BaGdF_5 grains (Figs. 12, 13). Similar effects to FGA_5 are observed for FGA_7.5 glass (Fig. 6), but the effect of BaGdF_5 crystallization is lower and the additional crystallization of $\text{Gd}_{9.33}(\text{SiO}_4)_6\text{O}_2$ occurs at higher temperature. Complete substitution of Al_2O_3 with

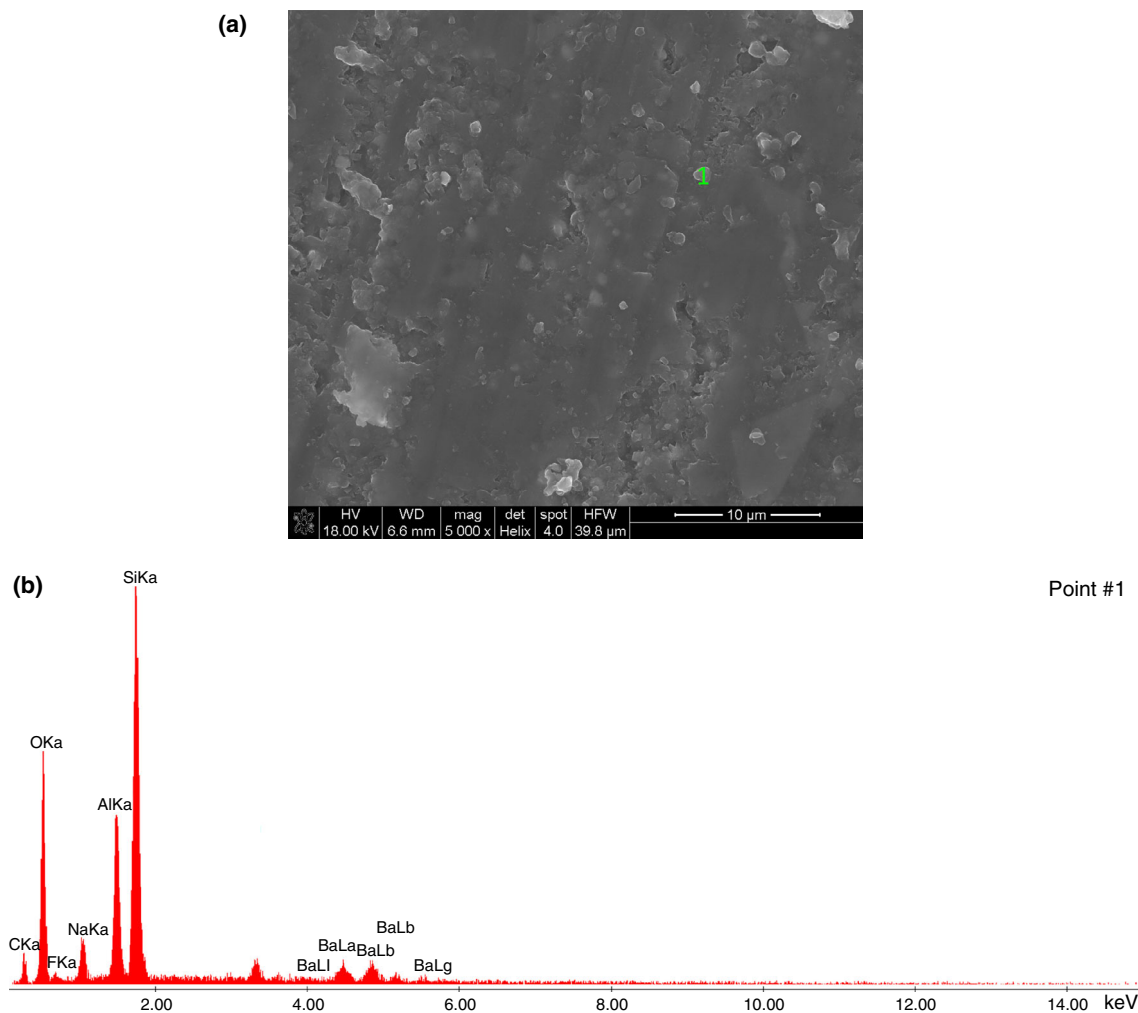


Fig. 10 SEM image (a) and EDS spectrum of FGA_0 after heat treatment at 900 °C for 12 h representing the point #1—crystallites of silicates (b)

Gd₂O₃ (FGA_10 glass) leads to change of the course of crystallization. Despite the 12 h heat treatment, intensity of corresponding BaGdF₅ peaks is very low (Fig. 7). Heat treatment at 880 °C for 12 h leads to small amounts of GdF₃ formation. At the same time, gadolinium silicate Gd_{9.33}(SiO₄)₆O₂ is formed. However, its ability to crystallization is lower than NaAlSi₃O₈.

XRD results show that introducing gadolinium oxide instead of Al₂O₃ affects the type of the fluorides to be formed and benefits the crystallization process. BaGdF₅ shows higher thermal stability than BaF₂. This observation may be important for obtaining of glass-ceramics containing low-phonon fluoride phase with high transparency.

SEM/EDS study

Figures 8 and 9 show the microstructure of FGA_0 sample after heat treatment at 750 °C for 2 h and 900 °C for

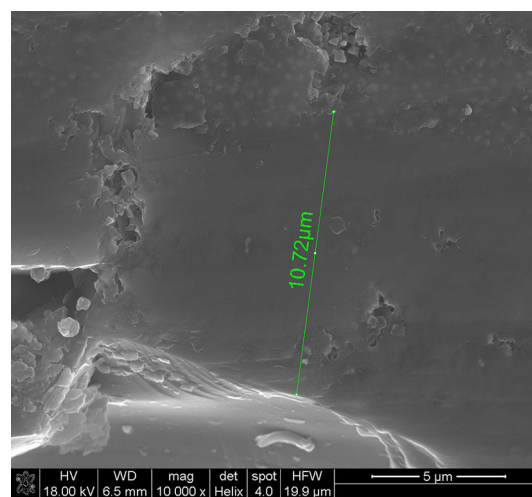


Fig. 11 SEM image of FGA_0 cross section after heat treatment at 900 °C for 30 min

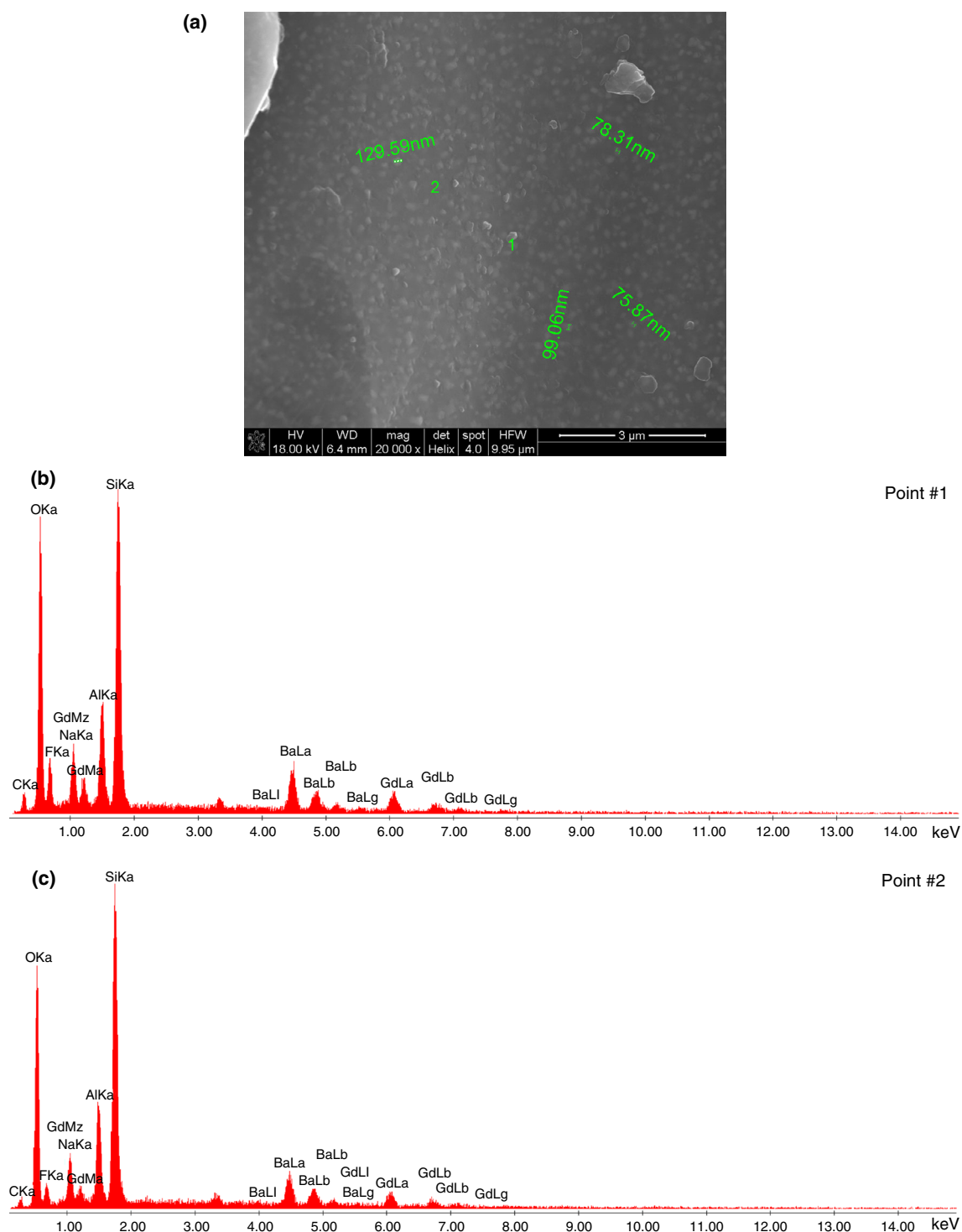


Fig. 12 SEM image (a) and EDS spectrum of FGA_5 after heat treatment at 770 °C for 2 h representing the point #1—crystallites of BaGdF_5 (b) and point #2—glassy matrix (c)

30 min. BaF_2 is visible in both samples. The crystallites are larger with much more spherical shape for higher temperature treatment.

The sample becomes mostly amorphous with increasing duration of heat treatment up to 12 h (Fig. 10). It is

confirmed by small thermal effects on DSC curves and lower intensity of peak on XRD pattern. EDS of the visible crystallites indicates the silicate phase formation. There is no sign of spherical BaF_2 crystallites that undergo dissolution.

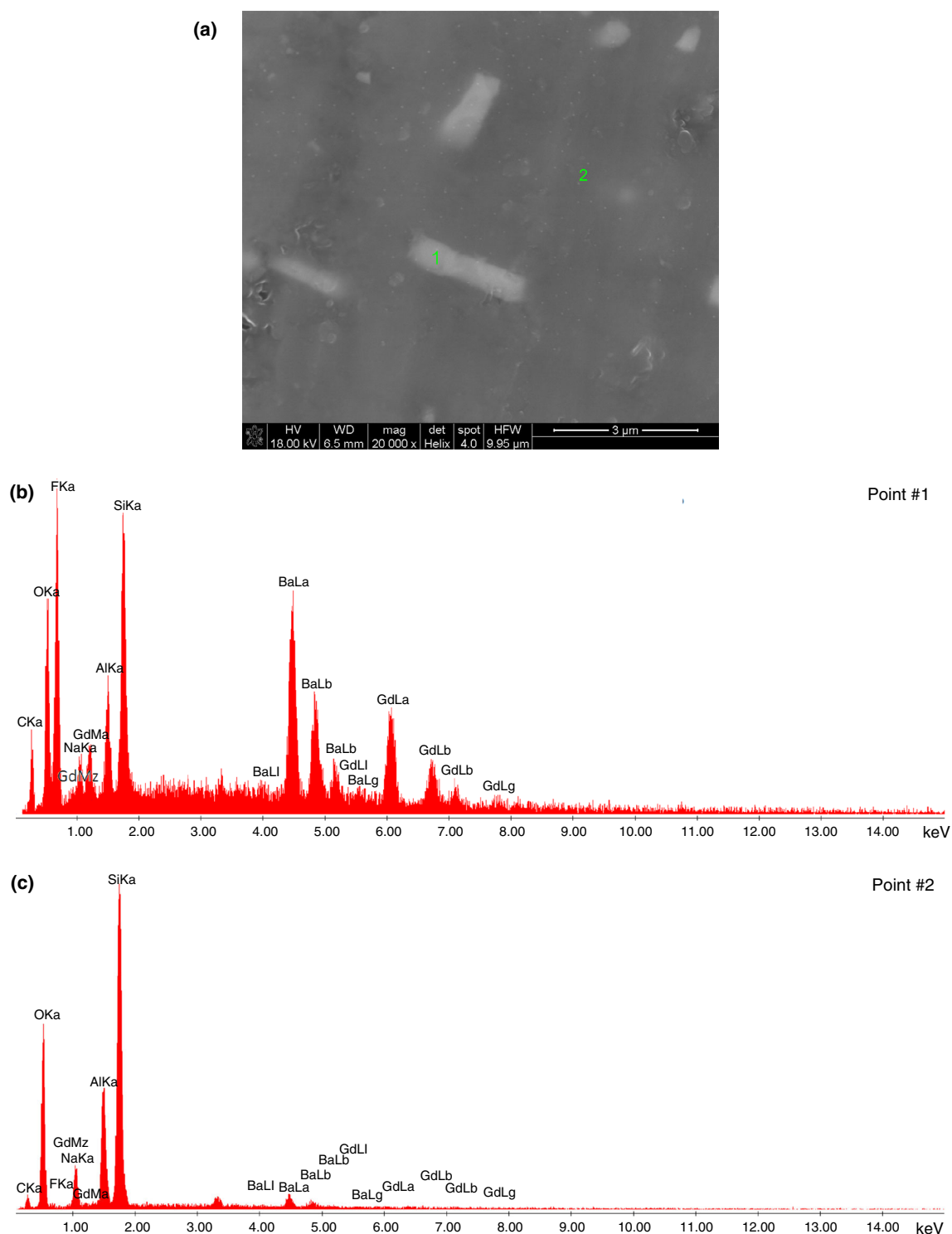


Fig. 13 SEM image (a) and EDS spectrum of FGA_5 after heat treatment at 900 °C for 12 h representing the point #1—crystallites of BaGdF₅ (b) and point #2—glassy matrix (c)

Figure 11 shows glass fracture near the sample surface. A difference in the cross section between the surface and the inside is visible. The distinct area of 10 μ m in width

with no visible BaF₂ crystallites is visible near the surface, unlike the inner part of the sample (upper part of the photograph). It may indicate a different chemical

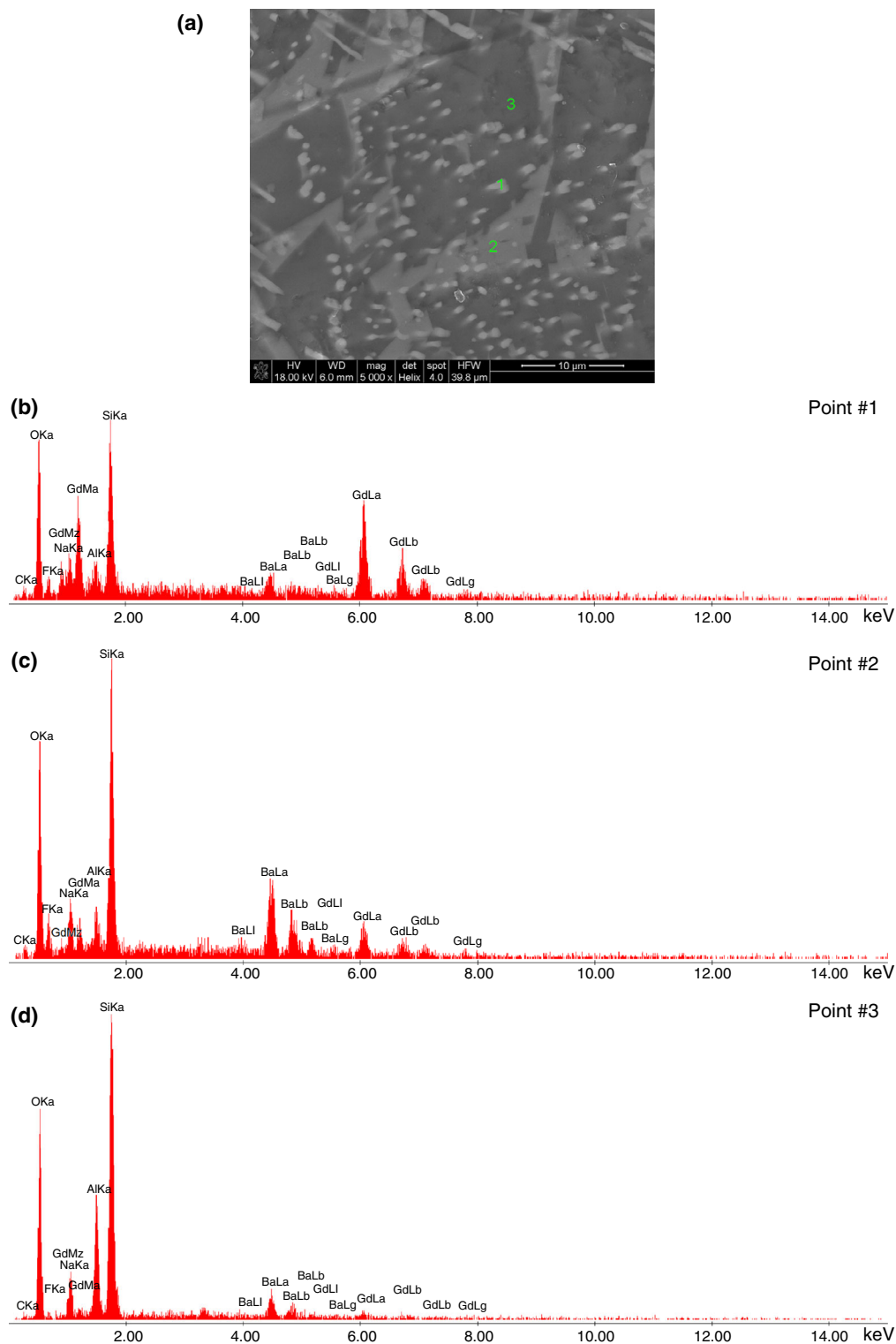


Fig. 14 SEM image (a) and EDS spectrum of FGA_7.5 after heat treatment at 1070 °C for 2 h representing the point #1—phase with higher concentration of Ga (b), point #2—phase with higher

concentration of Ba (c), point #3—phase with composition corresponding to $\text{Na}(\text{AlSi}_3\text{O}_8)$ (d)

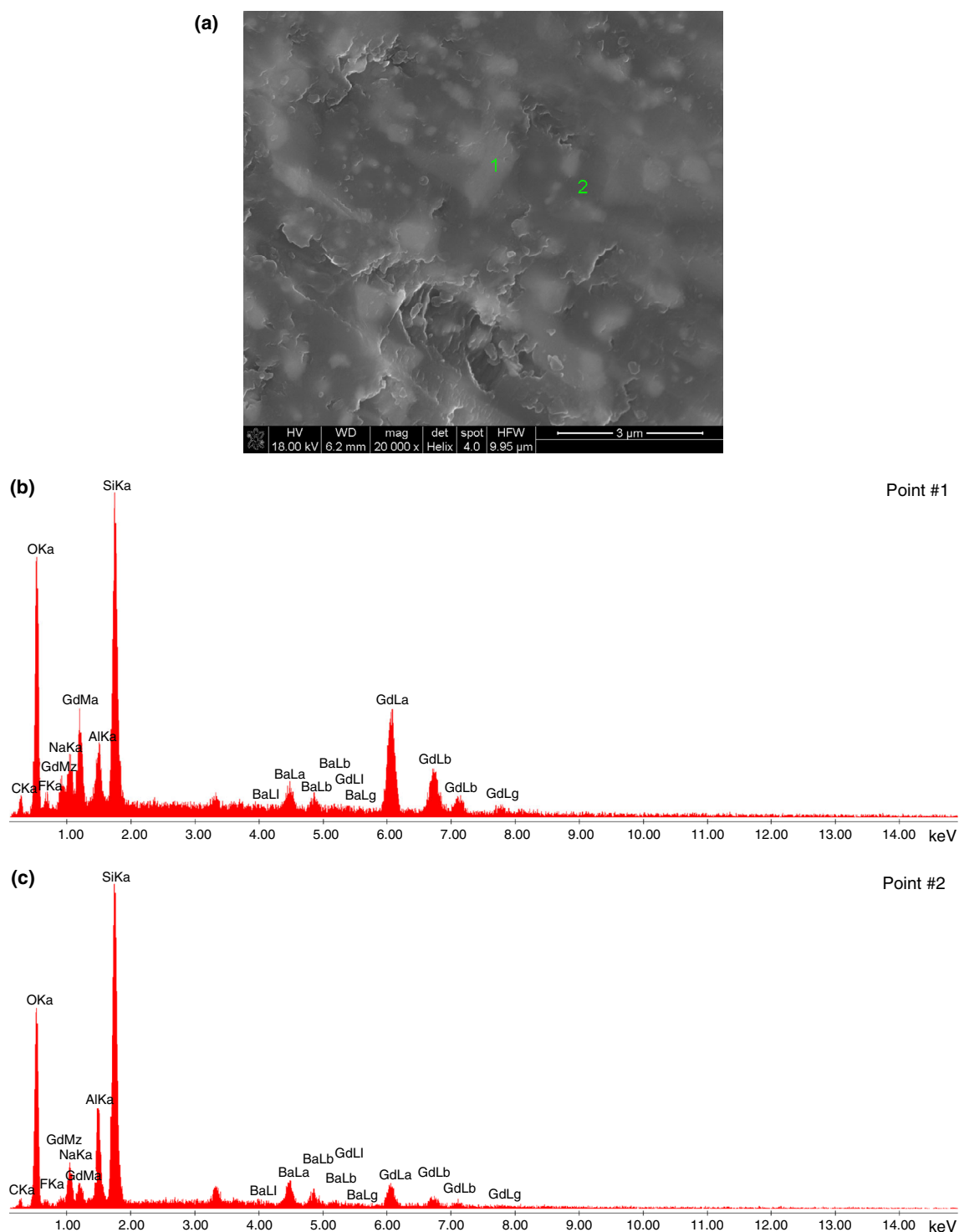


Fig. 15 SEM image (a) and EDS spectrum of FGA_10 after heat treatment at 880 °C for 12 h representing the point #1—crystallites of BaGdF₅ (b) and point #2—glassy matrix (c)

composition of the surface and the inside of the sample. Lack of fluoride phase formation in the surface layer may be a result of vaporization of fluorine during heat treatment.

A microstructure of FGA_5 sample after heat treatment at 770 °C for 2 h is presented in Fig. 12. Just comparing both heat-treated FGA_0 and FGA_5 samples, the difference in the size of crystallites can be observed. FGA_5

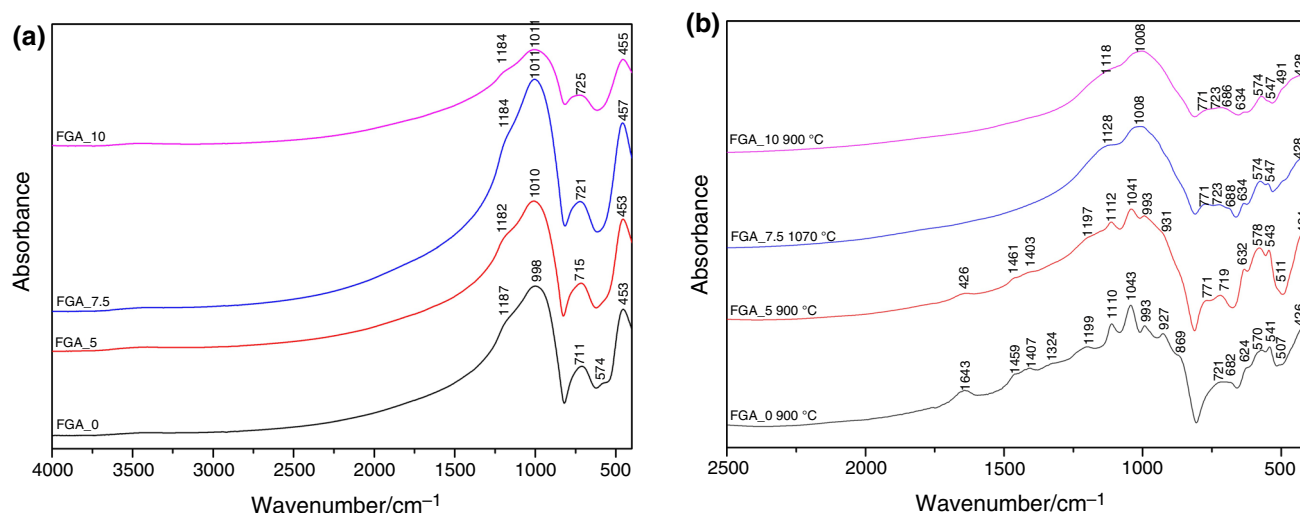


Fig. 16 FTIR spectra of as-made glasses (a) and glass-ceramic after 12 h of thermal treatment (b)

sample heated at even 20 °C higher temperature than FGA_0 sample shows significantly smaller crystallites, below 150 nm. However, the crystallites are well dispersed through the glass network and are not forming clusters in both cases.

SEM microphotograph reveals the formation of crystallites in the prism shape after 12 h of heating (Fig. 13). EDS analysis showed higher concentration of Gd, Ba and F atoms in this area, which may suggest a fluoride phase. XRD analysis confirmed formation of BaGdF_5 (Fig. 5) besides $\text{Na}(\text{AlSi}_3\text{O}_8)$ phase which is also visible as small crystallites.

Figure 14 presents microstructure of FGA_7.5 sample after treatment at the temperature 1070 °C for 2 h. The EDS analysis confirms the formation of three kinds of areas which may correspond to the formation of $\text{BaGdF}_5/\text{GdF}_3$, $\text{Gd}_{0.33}(\text{SiO}_4)_6\text{O}_2$ and $\text{Na}(\text{AlSi}_3\text{O}_8)$.

Figure 15 shows a microphotograph of FGA_10 sample after heat treatment at 880 °C for 12 h. Irregular areas with higher concentration of Gd precipitated in glassy matrix are observed (EDS point #1). Comparing these results with XRD analysis (Fig. 7), it can be concluded that they are mostly amorphous. The results correspond to the DSC analysis that shows lower values of ΔH .

FTIR study

FTIR spectra for as-made glasses are presented in Fig. 16a. Broad absorption lines confirm the amorphous nature of the samples. Increasing the fraction of Gd_2O_3 results in minor spectral changes. Replacing Al_2O_3 with Gd_2O_3 leads to a shift of the major band maximum toward higher wavenumbers. This band corresponds to stretching vibrations of tetrahedrons $[\text{SiO}_4]$ with various polymerization degree [22, 23]. Introducing Gd_2O_3 to the glass does not

shift the bands at 1187 cm^{-1} , which is connected with asymmetric Si-O-Si Q^4 and Si=O bond vibrations [24]. It can be an evidence that substitution of Al atoms with Gd does not cause silicate network depolymerization. On the other hand, the minor shift of 1000 cm^{-1} band associated with asymmetric vibrations of Si-O-Si Q^2 [25] is observed. The change in Si-O bond in the glasses doped with different content Gd_2O_3 can be assessed by the relationship between Si-O bond strength and effective frequency as reported in the literatures [26, 27]. The shift of the peak at about 1000 cm^{-1} may result the Si-O bond strength increase as the doping content of Gd_2O_3 increase. This effect may be explained by lower Gd-O bond strength, which leads to higher strength of $\text{Si-O}(\text{Gd})$ bond than $\text{Si-O}(\text{Al})$. To confirm the assumption a deconvolution analysis is needed. The band at 711 cm^{-1} is observed for the FGA_0 glass as a result of Si-O-Si bending vibration. The band shifts significantly and monotonously toward higher value of wavenumber when Gd content increases.

Figure 16b shows FTIR spectra for samples heated for 12 h at 900 °C (FGA_0, FGA_5, FGA_10) and at 1070 °C (FGA_7.5). For sample with 7.5 and 10 mol% Gd_2O_3 alone (spectra c and d), the spectra differ not much to the as-made glass spectrum. It indicates that the crystallization ability of $\text{Gd}_{0.33}(\text{SiO}_4)_6\text{O}_2$ is much lower than $\text{NaAlSi}_3\text{O}_8$. It should be noted that fluoride phases vibrations, due to the chemical nature of the bonds, are not active in IR spectroscopy [28, 29].

Conclusions

Replacing Al_2O_3 with Gd_2O_3 in the glass composition significantly influenced the crystallization behavior of fluoro-silicate glasses, both in terms of fluoride phase and

silicate network crystallization. The influence of the mixture of both oxides on crystallization was different than when we introduced them separately into the glass. Addition of Gd_2O_3 to the aluminosilicate glass increases the transformation temperature, at the same time decreasing ΔC_p and thermal stability ΔT . It also results in decrease of ΔH . The study indicates that Gd_2O_3 admixture significantly increases the activation energy of $\text{NaAlSi}_3\text{O}_8$ crystallization. Complete replacement of Al_2O_3 with Gd_2O_3 leads to $\text{Gd}_{0.33}(\text{SiO}_4)_6\text{O}_2$ formation, and Na-silicates crystallization is not observed. Due to Gd^{3+} ions participation in fluoride phases (BaGdF_5 , GdF_3) formation, crystallization of $\text{Gd}_{0.33}(\text{SiO}_4)_6\text{O}_2$ is impended, which was confirmed by our study. Thus, Gd_2O_3 can be used as a facilitating component for fabricating the low-phonon fluoride phases in the transparent glass-ceramics.

Acknowledgements This work was supported by AGH University of Science and Technology Department of Materials Science and Ceramics AGH number WIMiC No 11.11.160.365 in 2017. We would like to thank prof. M. Sitarz for his valuable comments.

Open Access This article is distributed under the terms of the Creative Commons Attribution 4.0 International License (<http://creativecommons.org/licenses/by/4.0/>), which permits unrestricted use, distribution, and reproduction in any medium, provided you give appropriate credit to the original author(s) and the source, provide a link to the Creative Commons license, and indicate if changes were made.

References

1. Reben M, Waclawska I, Paluszkiwicz C, Środa M. Thermal nad structural studies of nanocrystallization of oxyfluoride glasses. *J Therm Anal Cal.* 2007;88:285–9.
2. Chen D, Yu Y, Huang P, Lin H, Shan Z, Wang Y. Color-tunable luminescence of Eu^{3+} in LaF_3 embedded nanocomposite for light emitting diode. *Acta Mater.* 2010;58:3035–41.
3. Moos H. Spectroscopic relaxation processes of rare earth ions in crystals. *J Lumin.* 1970;1(2):106–21.
4. Cai J, Wei X, Hu F, Cao Z, Zhao L, Chen Y. Up-conversion luminescence and optical thermometry properties of transparent glass ceramics containing $\text{CaF}_2:\text{Yb}^{3+}/\text{Er}^{3+}$ nanocrystals. *Ceram Int.* 2016;42:13990–5.
5. Georgescu S, Voiculescu A, Matei C, Secu C, Negrea R, Secu M. Ultraviolet and visible up-conversion luminescence of $\text{Er}^{3+}/\text{Yb}^{3+}$ co-doped CaF_2 nanocrystals in sol-gel derived glass-ceramics. *J Lumin.* 2013;143:150–6.
6. Huang L, Jia S, Li Y, Zhao S, Deng D, Wang H, Jia G, Hua Y, Xu S. Enhanced emissions in Tb^{3+} -doped oxyfluoride scintillating glass ceramics containing BaF_2 nanocrystals. *Nucl Instrum Methods Phys Res Sect A.* 2015;788:111–5.
7. Li C, Xu S, Ye R, Deng D, Hua ZS, Zhuang S. White up-conversion emission in $\text{Ho}^{3+}/\text{Tm}^{3+}/\text{Yb}^{3+}$ tri-doped glass ceramics embedding BaF_2 nanocrystals. *Phys B Condens Matter.* 2011;406:1698–701.
8. Varshneya AK. Fundamentals of inorganic glasses. 4th ed. Sheffield: Society of Glass Technology; 2014.
9. Marquesi AR, Delben JRJ, Delben AS. Glass forming ability and thermal stability of oxyfluoride glasses. *J Therm Anal Cal.* 2009;96:403–6.
10. Atyia HE, Farid AS. Investigation and evaluation of the glass stability criteria for $\text{Se}_{60}\text{Ge}_{15}\text{X}_{25}$ ($\text{X}=\text{Sn}, \text{As}$) compositions. *J Therm Anal Cal.* 2017. doi:10.1007/s10973-016-6077-3.
11. Środa M. Effect of Er_2O_3 on thermal stability of oxyfluoride glass. *J Therm Anal Cal.* 2009;97:239–43.
12. Kissinger HE. Variation of peak temperature with heating rate in differential thermal analysis. *J Res Natl Bur Stand.* 1956;57:217–21.
13. Augis AJ, Bennett JE. Calculation of the Avrami parameters for heterogeneous for heterogeneous solid state reactions using a modification of the Kissinger method. *J Therm Anal Cal.* 1978;13:283–92.
14. Ozawa T. Kinetics of non-isothermal crystallization. *Polymer.* 1971;12:150–8.
15. Ozawa T. A new method of analyzing thermogravimetric data. *Bull Chem Soc Jpn.* 1965;38:1881–6.
16. Matusita K, Komatsu T, Yokota R. Kinetics of non-isothermal crystallization process and activation energy for crystal growth in amorphous materials. *J Mater Sci.* 1984;19:291–6.
17. Money BK, Hariharan K. Devitrification kinetics of bulk and pulverized sodium metaphosphate glassy phase. *Solid State Ion.* 2011;192:672–6.
18. Cheng CT, Lanagan M, Jones B, Lin JT, Pan MJ. Crystallization kinetics and phase development of $\text{PbO}-\text{BaO}-\text{SrO}-\text{Nb}_2\text{O}_5-\text{B}_2\text{O}_3-\text{SiO}_2$ -based glass-ceramics. *J Am Ceram Soc.* 2005;88:3037–42.
19. Karmakar P, Subudhi AK, Biswas K, Annapurna K. Crystallization kinetics analysis of BaF_2 and BaGdF_5 nanocrystals precipitated from oxyfluoride glass systems: a comparative study. *Thermochim Acta.* 2015;610:1–9.
20. Karpukhina NG, Werner-Zwanzinger JW, Kiprianov AA. Preferential binding of fluorine to aluminum in high peralkaline aluminosilicate glasses. *J Phys Chem B.* 2007;111:10413–20.
21. Matusita K, Sakka S. Kinetic study of non-isothermal crystallization of glass by thermal analysis. *Bull Inst Chem Res Kyoto Univ.* 1981;59:159–71.
22. Środa M, Paluszkiwicz C. The structural role of alkaline earth ions in oxyfluoride aluminosilicate glasses—Infrared spectroscopy study. *Vib Spectrosc.* 2008;48:246–50.
23. Roy BN. Infrared spectroscopy of lead and alkaline-earth aluminosilicate glasses. *J Am Ceram Soc.* 1990;73:846–55.
24. Partyka J, Sitarz M, Leśniak M, Gasek K, Jeleń P. The effect of $\text{SiO}_2/\text{Al}_2\text{O}_3$ ratio on the structure and microstructure of the glazes from $\text{SiO}_2-\text{Al}_2\text{O}_3-\text{CaO}-\text{MgO}-\text{Na}_2\text{O}-\text{K}_2\text{O}$ system. *Spectrochim Acta Part A.* 2015;134:621–30.
25. Tognonvi MT, Soro J, Rossignol S. Physical-chemistry of silica/alkaline silicate interactions during consolidation. Part 1: effect of cation size. *J Non-cryst Solids.* 2012;358:81–7.
26. Wang MT, Cheng JS, Li M, He F. Structure and properties of soda lime silicate glass doped with rare earth. *Phys B Condens Matter.* 2011;406:187–91.
27. Gafaar MS, Marzouk SY. Mechanical and structural studies on sodium borosilicate glasses doped with Er_2O_3 using ultrasonic velocity and FTIR spectroscopy. *Phys B Condens Matter.* 2007;388:294–302.
28. Kadlec F, Simon P, Raimboux N. Vibrational spectra of superionic crystals $(\text{BaF}_2)_{1-x}(\text{LaF}_3)_x$. *J Phys Chem Solids.* 1999;60:861–6.
29. Tressaud A, Poeppelmeier K. Photonic and electronic properties of fluoride materials. Cambridge: Elsevier; 2016.